Materials and Design 64 (2014) 355–359

Contents lists available at ScienceDirect

Materials and Design

journal homepage: www.elsevier.com/locate/matdes

Microstructural evolution and mechanical properties of friction stir welded joint of Fe–Cr–Mn–Mo–N austenite stainless steel

D. Wang, D.R. Ni, B.L. Xiao, Z.Y. Ma *, W. Wang, K. Yang

Shenyang National Laboratory for Materials Science, Institute of Metal Research, Chinese Academy of Sciences, 72 Wenhua Road, Shenyang 110016, China

ARTICLE INFO

Article history:
Received 8 June 2014
Accepted 29 July 2014
Available online 9 August 2014

Keywords:
Friction stir welding
Stainless steels
High nitrogen steels
Microstructure
Mechanical properties

ABSTRACT

2 mm thick Fe–18.4Cr–15.8Mn–2.1Mo–0.66N high nitrogen austenite stainless steel plate was successfully joined by friction stir welding (FSW) at 800 rpm and 100 mm/min. FSW did not result in the loss of nitrogen in the nugget zone. The arc-shaped band structure, consisting of a small amount of discontinuous ferrite aligning in the bands and fine austenite grains, was a prominent microstructure feature in the nugget zone. The discontinuous ferrite resulted from newly formed ferrite during welding and the remained ferrite, whereas the fine austenite grains were formed due to dynamic recrystallization of the initial austenite during FSW. The fine dynamically recrystallized grains in the nugget zone significantly increased the hardness compared to that of the base material. The strength of the joint was similar to that of the base material, with the joint failing in the base material zone.

1. Introduction

High nitrogen austenite stainless steel (HNS) with high strength, ductility and toughness is considered a group of promising structural materials for use in various industries [1]. Nitrogen as an alloying element not only is a strong austenite-stabilizing element, but also improves both the strength and fracture toughness of the alloy. More importantly, nitrogen can improve the local corrosion resistance of stainless steel, especially pitting and crevice corrosion resistance [2,3].

Wide industrial application of HNS depends on effective joining methods. The weldability of HNS is significantly reduced due to the addition of nitrogen element. It is hard to achieve defect-free HNS joints by conventional fusion welding techniques [4]. The nitrogen loss, welding defects and nitride precipitation in the welding process of HNS result in the loss of corrosion resistance and mechanical properties [5,6].

Friction stir welding (FSW) is a solid-state welding method which sees particular use in the aerospace and automotive industries [7]. During the welding process, a rotating tool with a specially designed pin and shoulder is inserted into the plates and traversed along the line of joint. Both localized heating and plastic deformation softens the material around the pin. The combination of tool rotation and translation results in movement of material from the front to the back of the pin, thereby producing a welded joint in the solid state. FSW was originally applied in joining low melting-point materials, such as Al, Mg and Cu alloys [8–10]. The solid-state nature of the FSW process is also applicable for welding steel without metallurgical changes or welding defects [7].

Recently, with significant progress in developing welding tools for joining high melting-point materials [11], a number of FSW investigations have been dedicated to join various steels [12–15]. In particular, for the austenite stainless steels, the sound joints of 304 steel could be achieved by FSW with the strength of the joints being equal to that of the base material (BM) [16]. However, for FSW of HNS, the investigations are quite limited.

Park et al. [17] conducted FSW of 6 mm thick Fe–23Cr–10Ni–6Mn–2Mo–0.2Si–0.53N austenite stainless steel on a single plate (technically friction stir processing) for the first time, in which the pin did not fully penetrate the welding plate. Although some defects existed in the nugget zone (NZ), the dynamically recrystallized austenite grains were observed and no loss of nitrogen was detected in the NZ. Miyano et al. [18] achieved defect-free FSW joints of 2 mm thick Fe–23Cr–0Ni–1Mo–1N austenite stainless steel. It was reported that the transverse strength of the joints was higher than that of the BM. However, the joint failed in the heat-affected zone (HAZ), which is attributed to the fact that the gauge length of the tensile specimens only included the NZ and HAZ.

From limited FSW investigations on HNS mentioned above, it is clear that the microstructure evolution of HNS during FSW and its effect on the mechanical properties of the joints are not well understood due to limited microstructural evidences and the

* Corresponding author. Tel./fax: +86 24 83978908.
E-mail address: zyma@imr.ac.cn (Z.Y. Ma).

http://dx.doi.org/10.1016/j.matdes.2014.07.063
0261-3069/

existence of welding defects as well as the usage of short-length tensile specimens [17,18]. Therefore, a deep FSW investigation on HNS is necessary by using defect-free joints and full gage length tensile specimens which include all microstructural zones.

In this study, a Fe–18.4Cr–15.8Mn–2.1Mo–0.69N–0.04C HNS was subjected to FSW investigation. The aim is to achieve a sound FSW joint of HNS and to elucidate the microstructural evolution of HNS during FSW and its effect on the mechanical properties of the joints.

2. Experimental details

2 mm thick Fe–18.4Cr–15.8Mn–2.1Mo–0.69N–0.04C austenite stainless steel plates were used in this study. The plates were hot-rolled at 1050 °C and then annealed at 1100 °C for 2 h. The plates were joined by FSW along the rolling direction at a welding speed of 100 mm/min and a tool rotation rate of 800 rpm. A PCBN tool with a shoulder 16 mm in diameter and a cylindrical pin 6 mm in diameter and 1.8 mm in length was used.

The nitrogen content of the BM and the NZ of the joint was analyzed by LECO TCH 600. Microstructural examination was carried out on the cross-section of the joints perpendicular to the welding direction. The specimen for optical microscopy (OM) was electrolytically etched in a solution of 10% oxalic acid, 90% water at 30 V. The phases in the joint were analyzed using X-ray diffraction (XRD) and electron backscattered diffraction (EBSD) techniques. The specimen for electron backscattered diffraction (EBSD) was prepared by electrolytic polishing with a 10% perchloric acid, 90% ethanol solution at 30 V. Thin foils for transmission electron microscopy (TEM) were prepared by twin jet-polishing in 10% perchloric acid, 90% ethanol solution cooled to −25 °C with liquid nitrogen at 15 V.

The Vickers hardness profile of the joint was measured on the cross-section along the mid-thickness of the welded plate. Tensile specimens with a gauge length of 40 mm and a width of 10 mm that includes all the microstructural zones were machined perpendicular to the welding direction with the NZ being in the center of the gauge.

3. Results and discussion

Fig. 1 shows the typical cross-sectional macrograph of the FSW joint. No macro-defects were detected in the joint, indicating that a sound HNS joint could be achieved at a welding speed of 100 mm/min and a tool rotation rate of 800 rpm by FSW. The nitrogen content of the NZ was 0.70 wt%, similar to that of the BM (0.66 wt%). This indicates that nitrogen was not lost during the FSW process. Similar to those reported in FSW Al alloys and austenite stainless steel [8,17], NZ, thermo-mechanically affected zone (TMAZ), HAZ were identified in the cross section of the joint. The NZ of the FSW HNS joint exhibited a basin shape.

Fig. 2 shows the hardness profile of the FSW joint on the cross section along the mid-thickness of the joint. The NZ exhibited hardness values of ~330 HV with a width of about 5 mm. Beyond the NZ, the hardness decreased gradually as the distance from the NZ increased. The hardness decreased to the level of the BM (~260 HV) in the regions about 8 mm from the NZ center.

Fig. 1. Macrostructure of FSW HNS joint perpendicular to the welding direction.

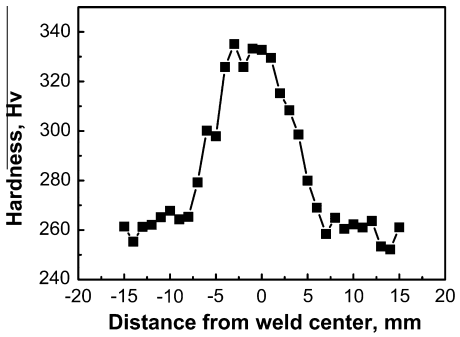

Fig. 2. Hardness profile of FSW HNS joint.

The yield strength (YS) and the ultimate tensile strength (UTS) of the joint were similar to those of the BM (Table 1), with the joint failing in the BM zone far away from the NZ (Fig. 3). This is consistent with the hardness distribution of the joint. This indicates that the sound joint of the HNS could be achieved by FSW. The fracture location of the joint in this study is different from that reported by Miyano et al. [18], where the FSW joint of 2 mm thick Fe–23Cr–0Ni–1Mo–1N plate failed in the HAZ, due to the usage of short-length tensile specimens that only included the NZ and HAZ in the gauge length. It is noted that the elongation of the joint was significantly lower than that of the BM. This is attributed to the heterogeneous hardness distribution on the cross section of the joint which resulted in the nonuniform deformation during the tensile process.

Fig. 4a shows the OM image of the BM perpendicular to the rolling direction. The BM exhibited an annealed coarse equiaxed grain structure with some fine grains at the grain boundaries of the coarse grains. The average grain size of the BM was determined to be ~39 μm. Some annealing twin boundaries were observed within some coarse grains. In addition, some δ ferrite with a strip shape was observed in the austenite matrix (marked by arrows). Although the BM was annealed at the austenite temperature, the δ ferrite formed during the hot-rolling process did not transform to austenite completely and some remained in the matrix. The existence of a small amount of ferrite is believed to be related to the process control during casting of the HNS. The element segregation during the casting process of this HNS resulted in that a small amount of δ ferrite retained in the matrix. This kind of ferrite was hard to remove completely during the following hot rolling and annealing process. The similar phenomenon was reported by Hong et al. [19]. The XRD profile, shown in Fig. 5, also indicated the presence of a small amount of the ferrite in the matrix. The relative content of the ferrite was calculated to be 5.6% using the relative area of the peaks between ferrite and austenite.

Fig. 4b shows the OM image of the HAZ, which has a microstructure similar to that of the BM. The microstructure of the HAZ was hardly affected by the thermal process of FSW. In the TMAZ (Fig. 4c), a distorted structure with the grains re-oriented was observed on the advancing side, similar to that of the FSW Al and steel joints [8,18].

Fig. 4d shows the OM image of the NZ close to the top surface of the joint. Some bands were observed in the matrix (marked by an arrow). Similar to other reports [14,17], the NZ was characterized by fine equiaxed recrystallized grains. The average grain size of

Table 1
Tensile properties of base material and FSW joint.

Sample	YS (MPa)	UTS (MPa)	El. (%)
BM	604	967	53.0
FSW	580	980	30.0

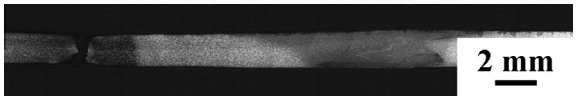

Fig. 3. Macroscopic image showing that transverse tensile specimen fractured at base material.

the NZ was 5.5 μm, much smaller than that of the BM. Few twin boundaries were observed within the grains due to the dynamic recrystallization during the FSW process. Moreover, the bands consisted of fine grains, similar to the results of Park et al. [17] and Reynolds et al. [20] in the FSW joints of 304 stainless steel. The fine grains in the NZ would increase the strength and the hardness compared to those in the BM.

To understand the structure of the bands, the NZ was observed from three planes. The various planes of the FSW joint were defined by the coordinate axis as shown in Fig. 6a. Fig. 6b presents the OM image in the *XZ* plane of the NZ. At the top of the *XZ* plane close to the shoulder, many bands were observed. However, at the zone near the bottom of the *XZ* plane, as marked by the arrow in Fig. 6b, the bands almost disappeared. In the *YZ* plane of the NZ (Fig. 6c), the bands were similar to those in the *XZ* plane. In contrast to those in the *XZ* and *YZ* planes, the bands in the *XY* plane were arc-shaped (Fig. 6d), similar to the onion skin that was the most prominent feature on the surface of the FSW joints [21].

In the FSW 304 stainless steel joint [22], the band structure consisting of fine grains and σ phases was also observed in the NZ. However, the nitrogen element would affect the phase transformation in steel and change the microstructure. Therefore, the bands in the NZ of the FSW joint of the HNS might be different from those of the 304 stainless steel.

Fig. 7a shows the TEM image of the BM. Similar to the OM image (Fig. 4a), the BM exhibited the annealed coarse grain structure. Furthermore, there were few dislocations within the grains. Fig. 7b shows the TEM image of the NZ. The fine grains were

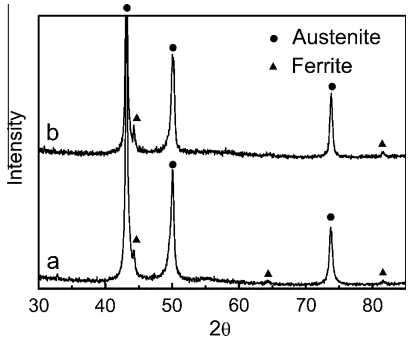

Fig. 5. XRD profiles of HNS: (a) base material and (b) nugget zone.

observed in this zone. Some dislocations, retained during the dynamic recrystallization process of FSW, were observed within the fine grains. Similar results were also reported in the FSW joints of Al alloys and steels [14,23]. However, the σ phase, which was reported in the fine grain bands in the NZ of FSW 304 stainless steel, was not found. Moreover, there were also no other phases in the matrix. This indicates that the microstructure of the bands in the NZ was different from that observed in the FSW joint of the 304 stainless steel [22].

The XRD profile of the NZ, as shown in Fig. 5, indicated that the ferrite was also present in the matrix, though it was not clearly observed under OM in Fig. 4d. The relative content of the ferrite in the NZ was 6.3%, slightly larger than that in the BM. The δ ferrite in the NZ came not only from the remaining ferrite in the BM, but also from the transformation of the austenite matrix during the FSW process. Miyano et al. [18] measured the temperature of the welding center during FSW of 2 mm thick Fe–23Cr–0Ni–1Mo–1N stainless steel at a tool rotation rate of 400 rpm and a welding speed of 100 mm/min. It was found that the temperature of the bottom surface in the NZ could reach 1050 °C. In this study, the

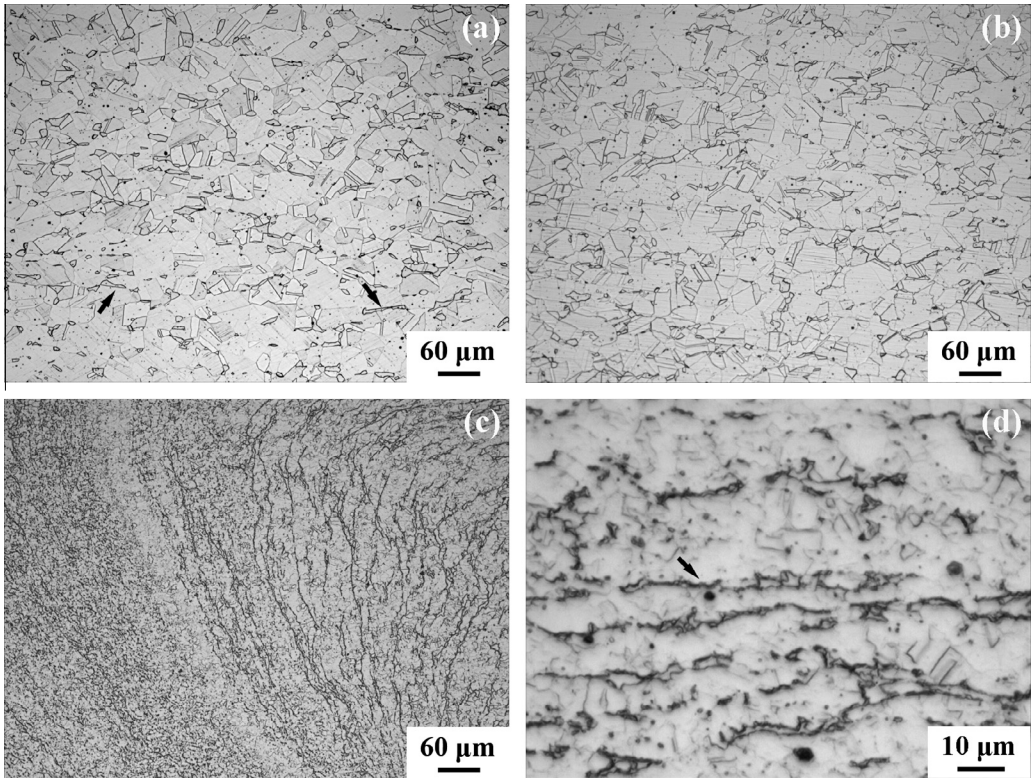

Fig. 4. Optical images of FSW HNS joint: (a) base material, (b) heat affected zone, (c) thermo-mechanically affected zone, and (d) nugget zone.

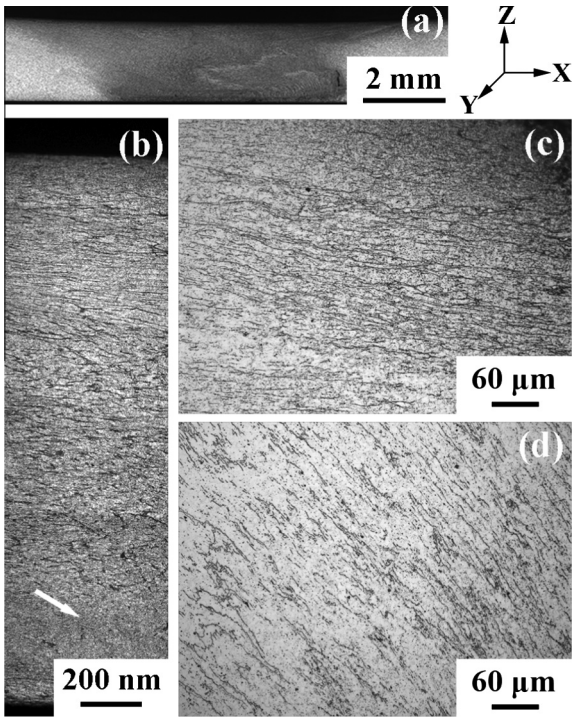

Fig. 6. Optical images of the bands in various planes of nugget zone: (a) macrostructure of the joint, (b) bands on *XZ* plane, (c) bands on *YZ* plane, and (d) bands on *XY* plane.

tool rotation rate was 800 rpm, higher than that used by Miyano et al. [18]. The higher rotation rate would result in a higher heat input, thus the NZ would experience a higher temperature.

It is well known that the actual temperature of the NZ is higher than that of the measured locations [7]. Therefore, the temperature of the NZ during the FSW process possibly exceeded the transformation temperature of austenite to δ ferrite, which was reported to be 1150 °C for this Fe–Cr–Mn–N steel [24]. On the other hand, it was reported that the δ ferrite could form in the NZ of austenite stainless steel, though the duration of the NZ at the peak temperature was only several seconds during FSW [22]. Therefore, it is possible for the δ ferrite to form in the NZ during the FSW process, and then the content of the ferrite increased slightly in the NZ compared to that in BM.

Fig. 8 shows the EBSD map of the NZ. The white grains were austenite and the gray grains were ferrite. The discontinuous ferrite grains and the fine austenite grains formed the band structure

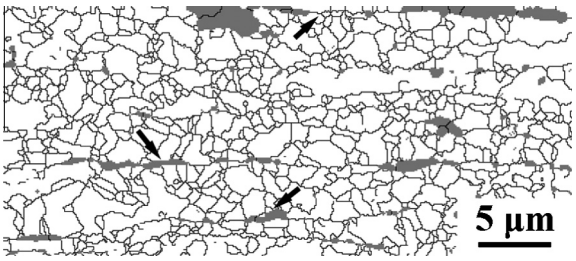

Fig. 8. EBSD maps showing grain boundaries and phase distribution of nugget zone (gray is ferrite, and white is austenite).

in the matrix (marked by black arrows), similar to that observed in Fig. 4d. Therefore, it can be presumed that the bands observed in Figs. 4d and 6 were the mixture of the ferrite grains and the fine austenite grains.

It was documented that the Mo element could promote the occurrence of dynamic recrystallization, because it retarded static recrystallization due to a solute drag effect [25]. Momenia et al. [25] reported that in the hot-compression process of a superaustenitic stainless steel, the dynamically recrystallized grains nucleated on the original grain boundaries, forming the fine recrystallized grains with the bulging grain boundaries due to the solute drag effect of Mo. Xu et al. [26] also found the fine dynamically recrystallized grains on the original grain boundaries during the tensile process at a high temperature in a high Mo austenitic stainless steel. Therefore, it could be deduced that the fine austenite grains were also formed during dynamic recrystallization process due to the effect of the Mo element in the matrix.

During the FSW process, the materials experienced severe plastic deformation with the rotating tool. The δ ferrite formed during FSW and the remaining ferrite of the BM would also flow with the matrix. The ferrite with the bcc crystal structure was more difficult to deform compared to the austenite with the fcc crystal structure at high temperatures. Therefore, the ferrite would follow the austenite flow during FSW and was distributed with discontinuous lace. In addition, the ferrite in the austenite matrix restrained the deformation of the matrix, especially the matrix between the discontinuous ferrite. The dynamic recrystallization was prone to occurring in these regions.

On the other hand, HNS has much lower stacking fault energy compared to the Al alloys, and therefore, the dynamic recrystallization more easily occurred in HNS than in the Al alloys [27]. Therefore, the fine austenite grains formed between the discontinuous ferrite. For thin sheets, the shoulder dominates the material flow in the NZ during the FSW process. Thus, the discontinuous ferrite

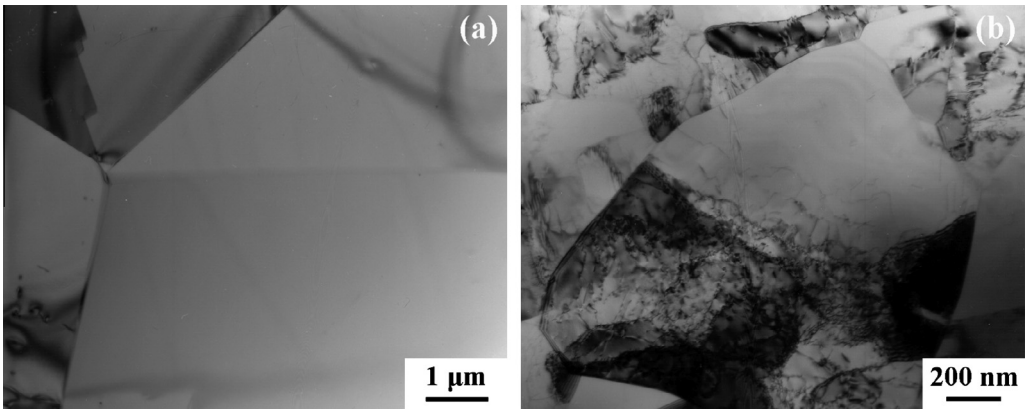

Fig. 7. TEM images of HNS: (a) based material and (b) nugget zone.

was distributed in the arc-shaped bands, similar to the onion skins on the surface of FSW joints. Moreover, more bands were observed on the top of the *XZ* plane where the matrix was prone to being affected by the shoulder.

4. Conclusions

In this study, the friction stir welding of 2 mm Fe–18.4Cr–15.8Mn–2.1Mo–0.66N–0.04C austenite stainless steel plates was carried out and the microstructure and mechanical properties of the joint were investigated. The following conclusions are reached.

(1) Sound FSW joint of 2 mm Fe–18.4Cr–15.8Mn–2.1Mo–0.66N–0.04C austenite stainless steel plates were successfully achieved at a welding speed of 100 mm/min and a tool rotation rate of 800 rpm. The nitrogen was not lost during the FSW process.
(2) The fine equiaxed recrystallized grains in the nugget zone increased the hardness of the nugget zone significantly. The strength of the joint was similar to that of the BM, with the joint failing in the BM zone.
(3) The arc-shaped band structure was the prominent microstructure feature in the nugget zone and it consisted of a small amount of discontinuous ferrite aligning in the bands and fine dynamically recrystallized austenite grains between the discontinuous ferrite.

Acknowledgments

This work was supported by National Natural Science Foundation, China (No. 51201163) and National Basic Research Program, China (No. 2012CB619101).

References

[1] Lo KH, Shek CH, Lai JKL. Recent developments in stainless steels. Mater Sci Eng, R 2009;65:39–104.
[2] Simmons JW. Overview: high-nitrogen alloying of stainless steels. Mater Sci Eng, A 1996;207:159–69.
[3] Wang ST, Yang K, Shan YY, Li LF. Plastic deformation and fracture behaviors of nitrogen-alloyed austenitic stainless steels. Mater Sci Eng, A 2008;490:95–104.
[4] Woo I, Kikuchi Y. Weldability of high nitrogen stainless steel. ISIJ Int 2002;42:1334–43.
[5] Kawahito Y, Mizutani M, Katayama S. High quality welding of stainless steel with 10 kW high power fiber laser. Sci Technol Weld Joi 2009;14:288–94.
[6] Nishimoto K, Mori H. Hot cracking susceptibility in laser weld metal of high nitrogen stainless steels. Sci Technol Adv Mater 2004;4:231–40.
[7] Mishra RS, Ma ZY. Friction stir welding and processing. Mater Sci Eng, R 2005;50:1–78.
[8] Zhang Z, Xiao BL, Wang D, Ma ZY. Effect of alclad layer on material flow and defect formation in friction-stir-welded 2024 aluminum alloy. Metall Mater Trans A 2011;42:1717–26.
[9] Xue P, Xiao BL, Zhang Q, Ma ZY. Achieving friction stir welded pure copper joints with nearly equal strength to the parent metal via additional rapid cooling. Scr Mater 2011;64:1051–4.
[10] Xie GM, Ma ZY, Geng L. Effect of Y addition on microstructure and mechanical properties of friction stir welded ZK60 alloy. J Mater Sci Technol 2009;25:351–5.
[11] Rai R, De A, Bhadeshia HKDH, Debroy T. Review: friction stir welding tools. Sci Technol Weld Joi 2011;16:325–42.
[12] Thomas WM, Threadgill PL, Nicholas ED. Feasibility of friction stir welding steel. Sci Technol Weld Joi 1999;4:365–72.
[13] Fujii H, Cui L, Tsuji N, Maedac M, Nakata K, Nogi K. Friction stir welding of carbon steels. Mater Sci Eng, A 2006;429:50–7.
[14] Chung YD, Fujii H, Ueji R, Tsuji N. Friction stir welding of high carbon steel with excellent toughness and ductility. Scr Mater 2010;63:223–6.
[15] Bilgin MB, Meran C. The effect of tool rotational and traverse speed on friction stir weldability of AISI 430 ferritic stainless steels. Mater Des 2012;33:376–83.
[16] Ishikawa T, Fujii H, Genchi K, Iwaki S, Matsuoka S, Nogi K. High speed-high quality friction stir welding of austenitic stainless steel. ISIJ Int 2009;49:897–901.
[17] Park SHC, Sato YS, Kokawa H, Okamoto K, Hirano S, Inagaki M. Microstructure of friction-stir-welded high-nitrogen stainless steel. Mater Sci Forum 2007;539–543:3757–62.
[18] Miyano Y, Fujii H, Sun Y, Katada Y, Kuroda S, Kamiya O. Mechanical properties of friction stir butt welds of high nitrogen-containing austenitic stainless steel. Mater Sci Eng, A 2011;528:2917–21.
[19] Hong CM, Shi J, Sheng LY, Cao WQ, Hui WJ, Dong H. Influence of hot working on microstructure and mechanical behavior of high nitrogen stainless steel. J Mater Sci 2011;46:5097–103.
[20] Reynolds AP, Tang W, Herold TG, Prask H. Structure, properties, and residual stress of 304L stainless steel friction stir welds. Scr Mater 2003;48:1289–94.
[21] Cui GR, Ma ZY, Li SX. Periodical plastic flow pattern in friction stir processed Al–Mg alloy. Scr Mater 2008;58:1082–5.
[22] Park SHC, Sato YS, Kokawa H, Okamoto K, Hirano S, Inagaki M. Rapid formation of the sigma phase in 304 stainless steel during friction stir welding. Scr Mater 2003;49:1175–80.
[23] Su JQ, Nelson TW, Mishra R, Mahoney M. Microstructural investigation of friction stir welded 7050-T651 aluminium. Acta Mater 2003;51:713–29.
[24] Wang ST. Ph.D. thesis mechanical behaviors and mechanisms of nitrogen effect of high nitrogen austenitic stainless steels, Graduate School of Chinese Academy of Sciences Beijing, China; 2008.
[25] Momenia A, Dehghania K, Keshmirib H, Ebrahimic GR. Hot deformation behavior and microstructural evolution of a superaustenitic stainless steel. Mater Sci Eng, A 2010;527:1605–11.
[26] Xu YR, Chen LS, Wang DY, Jin L. Flow behavior and evolution of microstructure during hot deformation for a high Mo stainless steel. J Mater Sci Technol 2000;16:341–4.
[27] Sato YS, Nelson TW, Sterling CJ. Recrystallization in type 304L stainless steel during friction stirring. Acta Mater 2005;53:637–45.